Highly chelating stellate mesoporous silica nanoparticles for specific iron removal from biological media

Paula Duenas-Ramirez, Caroline Bertagnolli, Roxane Müller, Kevin Sartori, A. Boos, Mourad Elhabiri, Sylvie Bégin-Colin, Damien Mertz

Highly chelating stellate mesoporous silica nanoparticles for specific iron removal from biological media

Paula Duenas-Ramirez[1], Caroline Bertagnolli[2], Roxane Müller[1], Kevin Sartori[1], Anne Boos[2], Mourad Elhabiri[3], Sylvie Bégin-Colin[1], Damien Mertz[1]

[1]Institut de Physique et Chimie des Matériaux de Strasbourg (IPCMS), UMR-7504 CNRS-Université de Strasbourg, 23 rue du Lœss, BP 34 67034, Strasbourg Cedex 2, France.
[2]Equipe de Reconnaissance et Procédés pour la Séparation Moléculaire (RePSeM), IPHC, UMR 7178 CNRS, Université de Strasbourg, ECPM, 25 rue Becquerel, 67087 Strasbourg Cedex 2, France
[3]Equipe de Chimie Bioorganique et Médicinale, Laboratoire d'Innovation Moléculaire et Applications (LIMA), UMR 7042, CNRS-ECPM-Université de Strasbourg-Université de Haute Alsace, 25 rue Becquerel, 67087 Strasbourg Cedex, France.

E-mail : damien.mertz@ipcms.unistra.fr

Abstract.

In this work, the design of a new generation of functionalized large pore silica nanoparticles is addressed for the specific removal of iron from biological environments. Herein, mesoporous silica with a large pore stellate morphology, denoted STMS, were grafted with the highly specific iron chelating agent desferrioxamine B, DFoB. The challenge of this work was the step by step elaboration of the nanoplatform and the evaluation of its chelating efficiency and selectivity. Hence, the controlled covalent grafting of DFoB specific iron chelator, was successfully achieved ensuring a high grafting rate of chelating ligand of 730 nmol·mg^{-1} (*i.e.*, 0.85 ligand·nm²). Furthermore, these highly chelating STMS silica were able to capture iron(III) stabilized with nitrilotriacetic acid (NTA) in solution at physiological pH with a fast kinetics (less than 30 minutes). For a stoichiometry 0.85:1 (FeNTA : DFoB), the STMS-DFoB nanoparticles allowed reaching capture capacity and efficiency of 480 nmolFe^{3+}/mg SiO_2 and 78%, respectively. Regarding the selectivity features of the removal process, studies were performed with two different media composed of various metal ions: (i) an equimolar solution of various metal cations and (ii) a Barth's buffer mimicking the brain solution composition. In both cases, the chelating STMS-DFoB showed a high selectivity for iron versus other ions at the same (Al^{3+}) or different valency (Na^+, K^+…). Finally, this work paves the way for new nanosystems for metal overload treatments as well as for future highly chelating nanoplatforms that can be used at the interface between depollution and nanomedecine.

Introduction

Among metallic pollutants, iron, even if less toxic than heavy metals, is a common constituent of groundwater and may induce taste and nuisance problems (discolouration, staining, deposition in distribution systems....)[1]. Another major problem with iron is overload in the body which induces strong health problems. In fact, every living organism feeds on iron, this metal being an essential micronutrient for oxygen transport under the hemoglobin form, furthermore, iron takes part in several metabolic processes such as DNA reparation[2]. Naturally, living organisms tightly regulate the homeostatic level of iron, but due to genetic dysregulations, iron overload can thus occur. Some examples, well-known by medical doctors, are linked to illness in the case of hemochromatosis, where the production of proteins like hepcidine and hemoglobin are not tightly controlled and this leads to dysregulation of iron homeostasis storage problems[3]. Acute iron poisoning[4] or medical treatments (*e.g.*, iron supplementation) in diseases such as β-thalassemia[5] can also lead to an iron overload status. To rescue this iron regulation machinery, one successful medical treatment described so far is the chelation therapy with desferrioxamine B (DFoB), a low-molecular weight molecule, engineered by microorganisms to ensure their iron(III) uptake. Excreted to their direct environment, these molecules, also termed siderophores, firmly bind ferric ions. DFoB, a representative member of this class of siderophores, is a natural linear trihydroxamate-based binder excreted by the bacteria *Streptomyces pilosus* that is known to display a high affinity for Fe^{3+} [6,7] (log $K_{Fe(III)DFoB}$ = 30; pFe = 26.5, with pFe = -log$[Fe]_{free}$ for $[Fe]_0 = 10^{-6}$ M and $[DFoB]_0 = 10^{-5}$ M at pH 7.4[8,9]). Due to this property, DFoB is very selective for Fe^{3+} as compared to others metal ions of biological interest: Cu^{2+} (log K_{CuDFoB} = 14.1; pCu = 11.2)[10], Zn^{2+} (log K_{ZnDFoB} = 10.1; pZn = 6.6)[11], Ni^{2+} (log K_{NiDFoB} = 10.9)[10] or Al^{3+} (log K_{AlDFoB} = 24.5)[9]. However, DFoB used in its free form in chelation therapy (*i.e.*, administered by blood transfusion) often presents several side effects in patients (*e.g.,* infections and respiratory or gastrointestinal problems) and a low time in the circulation system limiting its effect [12]. To avoid these problems, a first strategy consisted in substituting DFoB by other drugs such as deferiprone[13] or deferasirox[14] that are orally administered. However, these treatments are equal or less effective and still present several side effects.

In that context, an innovative alternative, which is proposed in this work, is based on the use of a biocompatible material support that is expected to increase the circulation time of the chelating drug and to ensure the selective capture of high iron amount. The development of smart nanoplatforms ensuring a strong complexation of ferric ions, and combining a high level of surface density with a size adapted to circulation in biological environments without aggregation behavior, is therefore promising for the efficient, selective and without side-effect removal of biological media. The challenge here is to find a support with a high specific surface area and chelating ligands to

anchor on this support without affecting their chelating efficiency and selectivity. Very few works have been reported on iron chelators grafted on a support. For instance, Liu et al**.** [15] described polymeric nanoparticles functionalized with DFoB for iron uptake in the frame of an Alzheimer treatment. Other groups, such as Farjadian et al.[16], investigated the iron capture by a silica support to treat iron overload in children using EDTA binder ligand. Indeed, the use of functionalized nanoparticles (NPs) for pollutant removal applications in biological environments has emerged recently as an important research topic.[17,18] These last years, there were several studies that reported the ability of organic and inorganic nanomaterials to ensure the removal of molecules or ions from different biological media. For example, Pratsinis, A. et al.[19] reported on liposomes used to remove ammonia from mice. Due to the delicate design and also a lower robustness of organic nanomaterials such as liposomes, researches are now mainly directed towards inorganic NPs.[20–25]

Among all these potential nanomaterials, mesoporous silica (MS) are particularly attractive and considered as one of the most versatile and successful adsorbents for the removal of environmental pollutants in recent years[26]. Due to their large specific surface area (*ca.* 500 $m^2.g^{-1}$), their cost-effective synthesis and the easiness of functionalization, these materials –functionalized or not– were applied as adsorbents or catalyst supports, but also for medical treatments as drug delivery vehicles[27–29]. Regarding the toxicity aspects, even if several questions remain about their long-term retention because of their slow biodegradability, they were approved by the FDA (Food and Drug Administration) which undoubtedly paves the way toward their use in some other specific biomedical treatments. For example, Fu and al. demonstrated a large circulation time of mesoporous silica (MS) by intravenous injection in mice experiments. The MS were mainly stored in spleen and liver, and finally successfully secreted by urine and feces[30]**.**

Herein, this work aims at developing a new generation of functionalized large pore silica NPs that could contribute to specific removal of iron in biological environments. Our approach consists in grafting large pore stellate mesoporous silica (STMS) NPs with a specific iron chelator, such as DFoB and evaluating the selective capture of iron(III). The benefit of these NPs design is the high surface area (*ca.* 500 $m^2.g^{-1}$) of STMS NPs and a suitable pore size (*ca*. 15 nm) that allow a high grafting rate of DFOB ligands (*ca.* 410 $\mu g.mg^{-1}$ or 730 $nmol.mg^{-1}$ STMS). In our group, we previously used such STMS as platforms either by grafting quantum dots in their pores or by "incorporating" a magnetic iron oxide core in STMS[37,38] allowing to form new multimodal nanomaterials for magnetic hyperthermia, MRI and fluorescence imaging applications. Here too, the design of large pore MS is highly desirable regarding depollution applications as compared to small pores. However, to the best of our knowledge, the reported strategies on silica supports mainly described non-specific ligands that can chelate together a broad range of heavy metallic species for environmental applications.[31–34] There is therefore an urgent need to develop approaches allowing to extract cations more selectively

for bioremediation in human organism or from biological environments, but only a few studies have been focused on this research topic so far.[35,36] In this work, STMS platforms are used for the first time for depollution applications.

To reach such a functionalized nanomaterial, several steps are necessary as pictured in **Scheme 1**. First, after STMS NPs synthesis by a surfactant mediated sol-gel process[37], a three step covalent binding allows us to efficiently graft DFoB at the surface of silica. Next, DFoB-STMS have been tested for iron(III) uptake properties in HEPES-buffered solutions (physiological pH). Nitrilotriacetic acid (NTA) is used as an auxiliary ligand of iron(III) to prevent its precipitation into insoluble iron(III) hydroxide species and affords a time stable 1:1 stoichiometric FeNTA complex (log K_{FeNTA} = 6.0(3) at pH 7.4 and log K_{FeNTA} ~15-16)[38,39]. The moderate stability of FeNTA ensures successful ligand exchange processes in aqueous solution with $DFoB_{grafted}$ (or DFoB-STMS). Next, the Fe(III) uptake capacities of the newly designed DFOB grafted nanosystems were investigated to get a deeper understanding of the kinetics and thermodynamic aspects of the ligand exchange between NTA and DFoB-STMS. At last, the selectivity of iron(III) uptake of DFoB-STMS with respect to other metal ions (mixture of relevant cations) was investigated as well. The aim of our work was to develop smart nanoplatforms with high efficiency and selectivity towards iron for metal overload treatments.

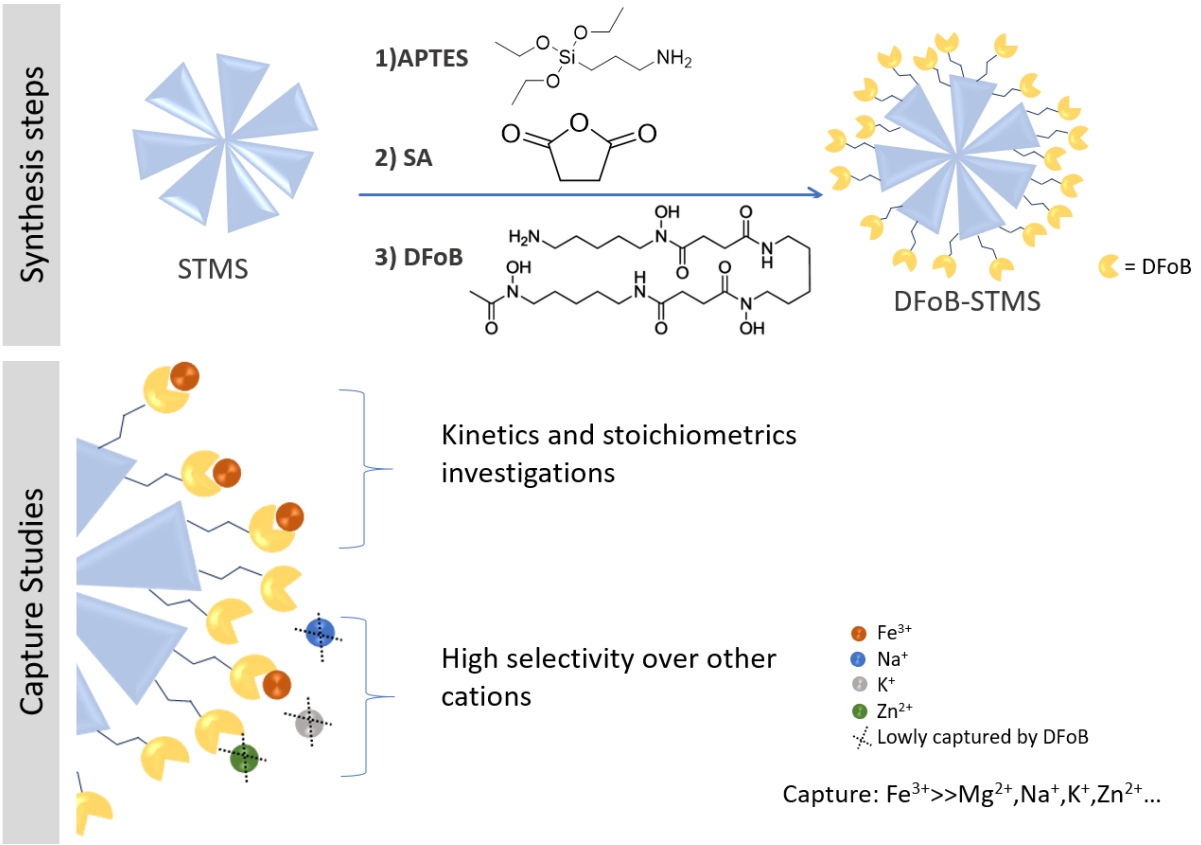

Scheme 1. General concept schematizing the grafting steps of DFoB on STMS NPs, and the subsequent applications of these materials for metal cation removal.

Experimental Section

Products. Cetyltrimethylammonium tosylate (CTATos, ≥98.0%), 2-amino-2-hydroxymethyl-1,3-propanediol (AHMPD, ≥99.9%), 3-aminopropyltriethoxysilane (APTES, 99%) and succinic anhydride (SA, ≥99%) were purchased from Sigma Aldrich; tetraethyl orthosilicate (TEOS, ≥99.0%) was purchased from Alfa Aesar. 1-ethyl-3-(3-dimethylaminopropyl)carbodiimide hydrochloride (EDC, >98.0%) was obtained from Tokyo Chemical Industry (TCI). Desferrioxamine B (DFoB) was obtained from Ciba-Geigy under its mesylate salt, while ammonium hydroxide sodium (NH_4OH) was purchased from Sigma Aldrich (puriss, p.a.). Fe(III) perchlorate hydrate ($Fe(ClO_4)_3 \cdot xH_2O$, Alfa Aesar (reagent grade), nitrilotriacetic acid trisodium salt, monohydrate (Fluka, prum, > 98%), 4-(2-hydroxyethyl)-1-piperazineethanesulfonic acid (HEPES, Sigma Life Science, ≥99.5%) and perchloric acid ($HClO_4$, normapur, 70% min), $AlCl_3 \cdot 6H_2O$ (99%) from Sigma Aldrich, different salts: NaCl from Carlo Erba (technical grade), $ZnCl_2$ (≥98%), $CaCl_2$ (≥97%) and $Ca(NO_3)_2 \cdot 4H_2O$ (≥98%) from Prolabo, $MgCl_2 \cdot 6H_2O$ (reagent grade) from Merck, KCl (>99%) from Labosi, $MgSO_4 \cdot 7H_2O$ (≥99.5%) from RP Normapur. All the products were used as received.

CAUTION! Perchlorate salts combined with organic ligands are potentially explosive and should be handled in small quantities and with the adequate precautions.[40]

Synthesis of stellate mesoporous silica nanoparticles (STMS). In a 500 mL flask, 3.80 g of CTATos, 0.436 g of AHMPD and 200 mL of distilled water were introduced and stirred at 80 °C up to complete dissolution (about 1h15). Next, 20.55 g (22 mL) of TEOS was added to the mixture, and stirred for 2h at 80 °C. A white precipitate of stellate mesoporous silica denoted STMS was formed and filtered under vacuum. The precipitate was washed three times with distilled water and dried overnight. The resulted powder was calcined at 600 °C for 6h to remove the CTATos surfactant. Next, around 5 g of this white powder was obtained and crushed with a mortar. 1 g of the crushed powder was added to 50 mL of ethanol in a centrifuge tube and sonicated during 10 minutes. About a half of the particles aggregated and fell to the bottom of the tube. The supernatant was separated and the precipitate was dried and then crushed again before adding it to the 50 mL of supernatant to disperse more particles. The suspension was treated with an ultrasound tip for a 20 minutes' cycle, and then the supernatant was isolated from precipitate.

Functionalization of STMS with aminopropyltriethoxysilane (APTES). 25 mL of STMS in ethanol (10 $mg \cdot mL^{-1}$) were added to 7 mL of ethanol in a tube with 1.2 mL of NH_4OH. The mixture was stirred for 5 minutes, and 5 mL APTES was added. The tube was mixed for 2 hours then separated in two and washed twice with 15 mL ethanol before being re-dispersed in 20 mL of ethanol.

Functionalization of STMS with carboxylic acids and grafting of Desferrioxamine B. A dispersion of the previously APTES-STMS obtained in DMF (15 mL) at 10 mg·mL^{-1} was added dropwise to a tube containing 30 mL of 0.1 M succinic anhydride (SA, 3 mol, 300 mg) in DMF to convert the amine into carboxylic functions. DMF must be anhydrous as water would hydrolyze the SA into succinic acid. The mixture was stirred for 24h, the resulting stellate MS NPs with carboxylic-function groups at their surface (STMS–COOH) were washed by centrifugation and redispersed in ethanol, repeated 3 times (20 mL). In the next step, 10 mL of COOH-STMS (10 mg·mL^{-1}) was dispersed in Na_2CO_3 buffer pH 7.2 (10 mg·mL^{-1}), and were brought in contact with DFoB (222.6 mg) bearing amino groups. A first addition of 159 mg EDC as activator agent was achieved and the tube was stirred for 1h. Then, 4 additional add-ons of EDC were performed each hour in order to activate the carboxyl functions left and the reactional media was stirred overnight before proceeding to several washings with water.

Iron capture experiments

***Fe(III) stock solutions*.** Fe(III) perchlorate stock solutions were freshly prepared in water at acidic pH (pH < 1.5) immediately before use and their concentrations were ascertained by UV-visible absorption spectrophotometry (ε^{240} = 4.16 x 10^3 M^{-1} cm^{-1} et ε^{260} = 2.88 x 10^3 M^{-1} cm^{-1})[41]. The glassware used was rinsed after each experiment with a hydrochloric acid solution to remove all traces of iron.

Iron nitroacetic (FeNTA) solution. 25 mL of a stock FeNTA solution (5 × 10^{-3} M) were freshly prepared by adding an aqueous solution of iron(III) (1 equiv.), whose concentration (3.8 × 10^{-2} M) was previously determined (*vide supra*). A slight excess of NTA (1.1 equiv.) with respect to iron(III) was always used to ensure complete complexation of iron(III) and avoid free ferric species in solution at pH = 7.4. The pH of the mixture was then raised to 7.4 with the help of a HEPES buffer (50 mM, pH 7.4).

***Kinetics investigations*.** 0.78 mg of the functionalized DFoB-STMS (equivalent to 0.52 mg STMS) were dispersed in 1.5 ml of a FeNTA solution (2.16·x 10^{-4} M) to ensure a stoichiometric amount at 0.85:1 of FeNTA with respect to $DefoB_{grafted.}$This solution was stirred over different reaction times (from 30 min to 1 day) and then centrifuged at 10 000 g for 10 minutes. The STMS-DFoB-Fe were washed 2 times with 1 mL of the HEPES buffered solution. The supernatants were then analyzed using UV-visible absorption spectrophotometry. An excess of free DFoB was added to the supernatant to ensure complete complexation of the unreacted FeNTA and the corresponding Fe(III) concentrations were evaluated from the absorbance measurement at 430 nm (LMCT absorption band of FeDFoB at 430 nm, ε^{430} = 2950 M^{-1}·cm^{-1})[7].

Thermodynamic investigations. 0.78 mg of the functionalized DFoB-STMS (equivalent to 0.52 mg STMS) were dispersed in 1.5 ml of a FeNTA solution whose concentration was varied from 4.3 x 10^{-5}

M to 4.3 x 10^{-4} M to ensure a variable stoichiometric amount in the range 0.17-1.7 :1 of FeNTA with respect to $DFoB_{grafted}$. The mixture was stirred during 30 min and centrifuged at 10 000 g for 10 minutes. The nanoparticles were then washed twice with 1 mL of the HEPES buffered solution. The supernatants were analyzed using UV-visible absorption spectrophotometry using the same protocol than that used for the kinetic study (see above).

Fe(III) selectivity of the DFoB-STMS. These experiments were conducted under two different conditions. In a first serie, the DFoB-STMS NPs (7.7 mg of DFoB-STMS, equivalent to 5.1 mg STMS) were subjected to a HEPES buffered solution (13.2 mL) containing FeNTA (0.27 mM) containing several metal salts of interest used at same concentration: $CaCl_2$, $ZnCl_2$ and $MgCl_2$. Na^+ cation was also used at 1.159 mM, a higher concentration than other ions because a NaOH solution (2 M) was necessary to fix the pH of the HEPES solution. In the second approach, 7.7 mg of the DFoB-STMS NPs were dispersed in a Barth's buffer[42]. This medium was reported to mimic the extracellular brain ionic composition (NaCl 88 mM, KCl 1 mM, $MgSO_4$ 0.82 mM, $NaHCO_3$ 2.4 mM, $CaCl_2$ 0.91 mM, $Ca(NO_3)_2$ 0.33 mM adjusted at pH 7.4 with a HEPES buffered solution at 10 mM). For these two types of experiments, the reaction mixtures were stirred for 30 min, centrifuged and the NPs were washed twice with the HEPES buffered solution. The elements content of the supernatants was analyzed by Inductively Coupled Plasma-Atomic Emission Spectroscopy (ICP-AES).

Characterizations techniques

Transmission Electron Microscopy (TEM and TEM-EDX). A transmission electron microscope JEOL 2100 high-resolution microscope operating at 200 kV was used to characterize the size and morphology of the STMS silica. EDX was used to investigate the presence of Fe and Si elements.

Dynamic Light Scattering (DLS) and Zeta Potential (ZP). The zetasizer Nano ZS from Malvern DLS was used to characterize the properties of colloidal suspensions: the hydrodynamic diameter and the dispersity in size in intensity mode. Measurements of surface Zeta potential were performed to get insights into the surface charge of the particles.

Thermal Gravimetric Analysis (TGA). TGA was performed on a TA SDT 600 instrument to measure the loss mass of the sample when the temperature changed. With these results, the amount of organic compound grafted on functionalized inorganic STMS nanoparticles can be quantified.

The Brunauer-Emmett-Teller (BET) nitrogen (N_2) adsorption/desorption isotherms. To characterize the porosity of the silica nanoparticles, adsorption and desorption of nitrogen isotherms were measured on a ASAP 2420 V instrument with around 100 mg of STMS nanoparticles. The Brunauer-Emmett-Teller (BET) method was used to calculate the surface area, and the pore size was obtained according to BJH (Barrett, Joyner and Halenda) model.

UV-visible Absorption Spectrophotometry. For the FeNTA supernatants analyses, 1.1 eq of free DFoB in solution ($DFoB_{free}$) was added to 1 ml of supernatant solution to ensure complete complexation of iron(III). The color changes from light yellow to orange (confirming the NTA-DFoB ligand exchange). The solutions were analyzed (from 200 to 800 nm) with quartz optical cell (Hellma) using either a CARY50 Probe Varian absorption spectrophotometer or an Agilent CARY5000 absorption spectrophotometer maintained at 25.0 (2) °C (Lauda E200 thermostat) between 200 and 800 nm.

Inductively Coupled Plasma-Atomic Emission Spectroscopy (ICP-AES). Iron concentrations of initial and extracted solutions were measured using ICP-AES with a Varian 720 ES instrument. Similarly, other cations: Al^{3+}, Zn^{2+}, Cu^{2+}, Ca^{2+} or Na^{+} from the selectivity study were also dosed by ICP-AES.

CHN elemental analysis. The amino groups grafted on the silica surface (APTES-STMS) were analyzed using a Flash 2000 / ThermoFisher CHNS analyzer.

Results and Discussion

Synthesis and characterization of stellate mesoporous silica nanoparticles (STMS NPs) suspensions

Mesoporous silica (MS) NPs having a stellate morphology (STMS) were prepared through the sol-gel procedure using the structure directing agent CTATos as described previously[37,43]. Low magnification TEM image in **Figure 1.A** shows a narrow size distribution of 95±6 nm of nicely structured STMS with a homogenous stellate morphology. A magnified image (**Figure 1.B**) clearly shows the stellate pore morphology. The porous properties (*i.e.*, surface area, pore size, pore volume) of the STMS were investigated by BET-nitrogen adsorption (**Figure S1**). In a typical sample, nitrogen adsorption isotherm provided a surface area S_{BET} of *ca*. 498 $m^2 \cdot g^{-1}$ associated with a pore size of 16 nm. These results were consistent with those of the literature by comparing the STMS obtained from Zhang et al.[44] having a surface area S_{BET} of 590 $m^2 \cdot g^{-1}$ for particles of 130 nm and a pore size close to 17 nm. The STMS were then dispersed in ethanol or in water (pH=7) and formed excellent colloidal suspensions in those solvents with hydrodynamic diameters (Dh) of *ca*. 164 and 141nm, respectively (**Figure 1.C**). This colloidal stability is very favourable to a further homogenous functionalization of the NPs. The slightly larger mean hydrodynamic diameter of the STMS particle suspensions by comparison with the mean TEM diameter is attributed to the solvation shell and the inherent effects of NPs distribution in liquid suspensions. Zeta potential (ZP) measurements as a function of the pH in water were also performed (**Figure 1.D**). The ZP values were found to decrease from 1.8 mV at pH= 1.5 to -15 mV at pH=7.2 and the pH range beyond. The isoelectric point (IEP) of the STMS in water was found at *ca.* pH = 4 which is in agreement with such silica nanomaterialsI IEP[45].

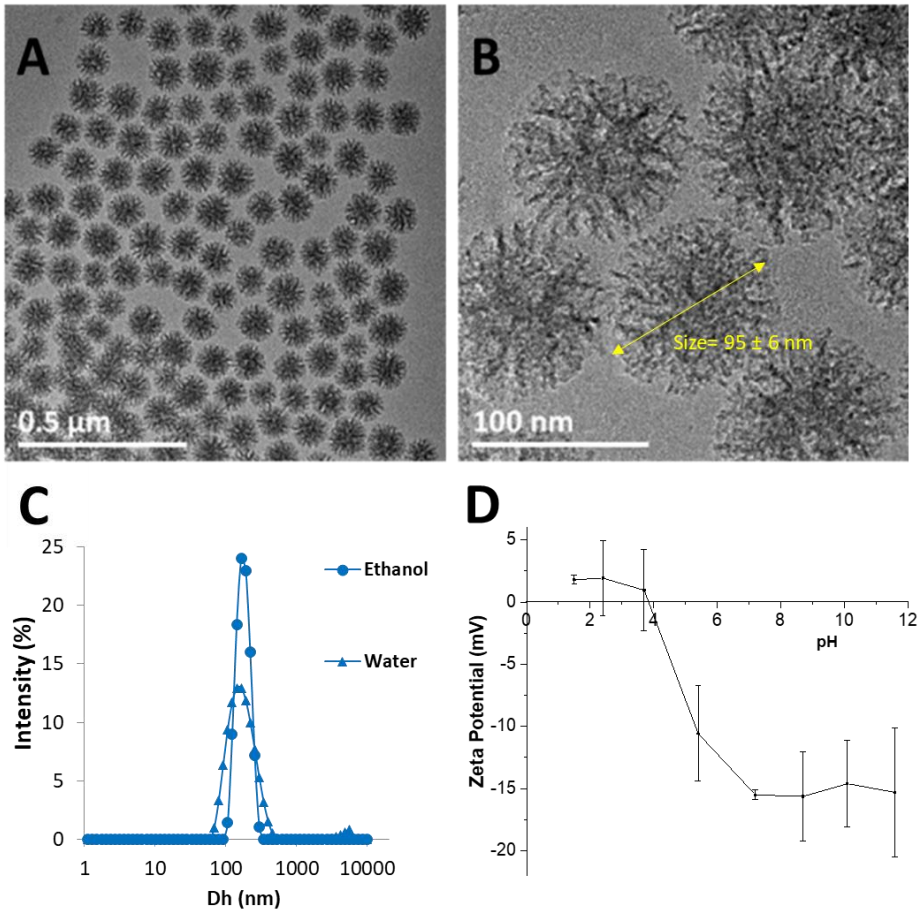

Figure 1. TEM images of STMS at (A) low and (B) high magnification. (C) DLS size distributions in intensity mode in water and in EtOH of the STMS. (D) ZP curve of the STMS in water *versus* pH.

Silica surface modification with Desferrioxamine (DFoB) ligand

The DFoB grafting at the silica surface requires three surface modification steps as shown in **Scheme 2**. The first one corresponds to the surface modification with aminopropyltriethoxysilane (APTES) by a condensation reaction in ethanol. In the second step, the amine groups of STMS are transformed into carboxylic acid functions using succinic anhydride (SA) and finally, those carboxylic groups are activated with 1-ethyl-3-3-dimethylaminopropylcarbodiimide hydrochloride (EDC) to react with the terminal amine function of the DFoB ligand.

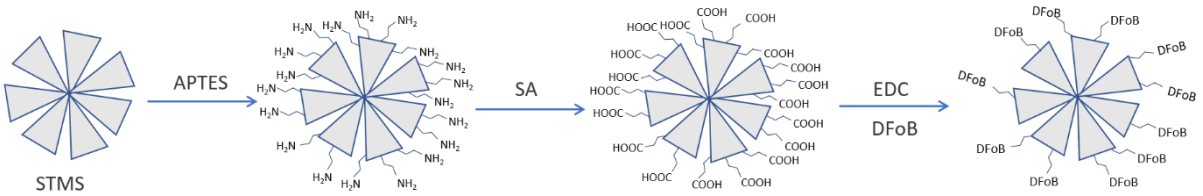

Scheme 2. Scheme describing the grafting of DFoB on STMS. It involves the introduction of carboxylic groups after reaction with APTES-STMS. A last step consists in coupling the EDC-activated carboxylic functions with the amine group of DFoB.

The grafting of APTES onto bare STMS surface to introduce amine terminal functions was obtained via the well-known procedure of silanization. The reaction is done in ethanol where the STMS particles are well dispersed in presence of ammoniac (Stöber-like conditions)[46] to form a NH_2 layer. As the grafting occurs, the surface of STMS is modified and the zeta potential value at same pH (7.2) increased from -15.5 mV to +20.3 mV. The charge reversal and positive value obtained after the reaction is consistent with the presence of ammonium groups of APTES grafted on the STMS. TGA was performed to quantify the organic content of these samples. In **Figure 2**, for both samples, STMS and APTES-STMS, a first weight loss was observed at 100°C, which was attributed to evaporation of solvent trapped inside the pores, even though the samples are dried before the measurements. For STMS (blue curve), a continuous weight loss is observed between 200 and 700 °C, and corresponds to the dehydroxylation of the silicate frameworks[44]. For APTES-STMS, several additional weight losses between 350 °C and 530 °C are linked to the burning of organic molecules grafted on the STMS. The grafting rate, previously defined as the amount of APTES grafted versus the mass of STMS, was then calculated to be at about 129 $\mu g_{APTES} \cdot mg_{SiO2}^{-1}$ (weight loss 11%,), which corresponds to a concentration of 2.9 amino functions per nm² **(Figure S2** and **Table S1** for the calculation method). Elemental analysis of C, H and N conducted to a grafting rate of 2.7 NH_2 functions·per nm² (**Table S2**) which is in the same range than TGA results. Furthermore, grafting rate is close with these of Schiestel et al. who reported 1.8 amino functions per nm² [47]. Therefore, the grafting of APTES was successfully completed ensuring a good coverage of the STMS NPs surface with amino functions.

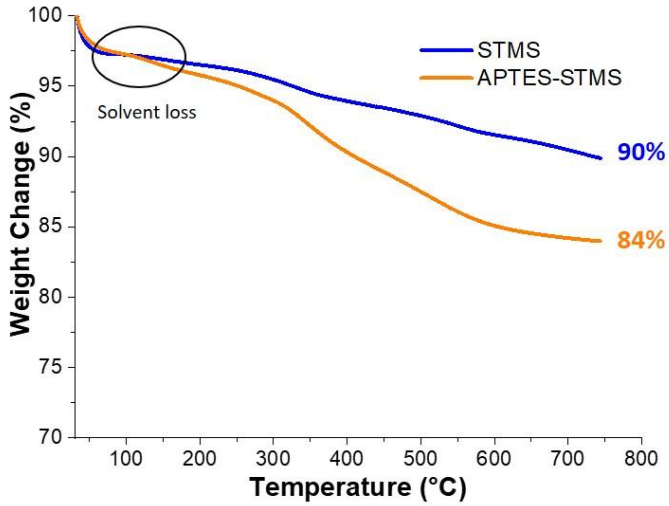

Figure 2. TGA curves of STMS (blue) and APTES-STMS (orange).

The introduction of carboxylic groups was performed by reacting the amine functions of APTES-STMS with succinic anhydride (SA) in DMF. The carboxylic acid groups were generated by a ring opening reaction between the amine groups and the SA cycle. The formed COOH-STMS bonds were characterized by TGA, FTIR and ZP measurements. TGA data indicated a weight loss of 17.5 wt% for the APTES and COOH organic layers (grey curve) which corresponds to 6.6 wt% specifically for the COOH grafts on STMS (**Figure 3.A** and **Table S1** for the calculation method) (values after solvent loss substraction). This allowed to calculate a grafting rate of 84 µg·mg^{-1} for COOH groups on STMS which after calculations correspond to a surface density of *ca*. 1 COOH functions·per nm², suggesting that *ca.* a third of amine functions have reacted with SA. Moreover, these results are consistent with the values obtained by An et al.[49] FTIR analysis of COOH-STMS and STMS allow evidencing the COOH group vibrations at 1548 and 1722 cm^{-1} attributed to the stretching and bending vibrations of the carboxyl group (**Figure S3**). With regard to the surface charge measured at pH 7.2 at each critical steps of the functionalization **(Figure 3.B)**, the inversion of the surface charge values is clearly demonstrated along the different grafting steps: bare (ZP= -13.5 mV); APTES (ZP = + 20.3mV); COOH modified STMs (ZP = -23 mV) which is perfectly consistent with the incorporation of deprotonated carboxylic functions (e.g., pK_a = 4.9 for propionic acid) at the silica surface.

Next, DFoB was grafted onto the COOH-STMS NPs: the continuous activation of the carboxylic groups of the COOH-STMS was achieved by a home-made procedure where sequential additions of EDC reagents are achieved every hour in the presence of DFoB in $NaHCO_3$ buffer at pH 7, with the aim of optimizing the reaction with the amine groups of the DFoB. Thus, coupling reaction of DFoB is carried out continuously throughout the defined reaction time. In the last activation step with the EDC reagent, the reaction mixture was stirred overnight. TGA analysis (**Figure 3.A,** DFoB yellow curve and

Table S1 for the calculation method) allowed determining a grafting rate of about 410 µg of DFoB per mg of STMS (730 nmol·mg^{-1}) corresponding to 0.85 ligand/nm².

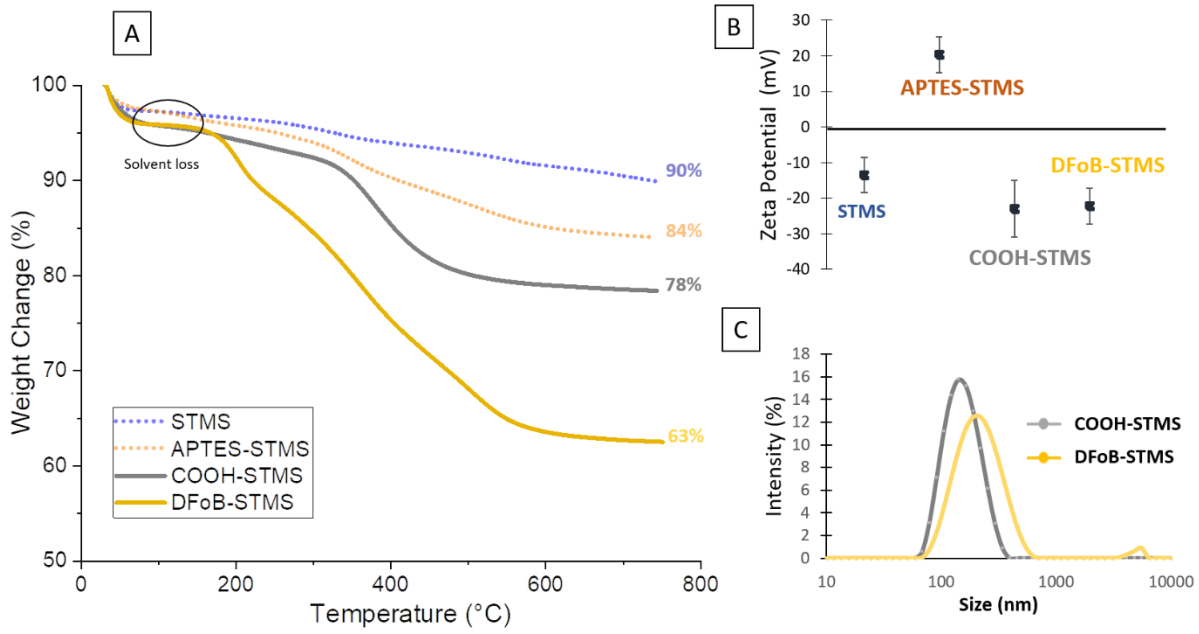

Figure 3. A) TGA and B) ZP of STMS (blue), APTES-STMS (orange), COOH-STMS (gray) and DFoB-STMS (yellow). TGA of STMS (blue) and APTES-STMS (orange) from Figure 2 were represented in dotted lines to highlight the surface modification, step by step.C) DLS size distribution of COOH-STMS (gray) and DFoB-STMS (yellow).

The colloidal stabilities of COOH-STMS and DFoB-STMS (**Figure 3.C**) were investigated by DLS measurements in HEPES buffered solution (50 mM, pH 7.2). The data demonstrate that the COOH-STMS suspensions display a good colloidal stability with an average hydrodynamic size of *ca*. 164 nm that can be explained by the strong electrostatic repulsions ensured by the terminal carboxylate functions in agreement with the the zeta potential value (*ca.* -23 mV) of the COOH-STMS. After functionalization by DFoB, the high colloidal stability is maintained with an average hydrodynamic size of ca. 220 nm (DLS, **Figure 3.C**) in buffered solution (HEPES 50 mM, pH 7.2). This striking result can be explained by the structure of DFoB, which contains hydrophilic fragments that probably contribute to the strong colloidal stability by introducing steric repulsion.

Fe(III) uptake by DFoB-STMS: kinetic and stoichiometric parameters

The major objective of this work was to evaluate the ability of the DFoB-STMS NPs to firmly chelate ferric ions in solution and to adress their use as innovative nanoplatforms for the elimination of toxic ions from the human body. A critical point is thus to demonstrate that the immobilization of DeFoB on the silica surface does not affect its chelating efficiency. As the iron capture would have to be

performed in biological media such as blood, we have to consider the iron speciation in such media as iron cations in water easily form hydroxides. In fact, at physiological conditions (pH 7.4), iron(III) does (almost) not exist as free cations in water: the equilibrium concentration of free Fe^{3+} is only about 10^{-18} M ($K_{sp}(Fe(OH)_3)$ = 2.6 x 10^{-39})[51]. To maintain its solubility and homeostasis under physiological conditions, iron(III) is constantly bound to proteins (*e.g.*, hemoglobin, transferrin) or to low molecular weight moderate chelators such as citrates (*i.e.*, the non-proteinic bound iron is called "labile iron pool"). Therefore, an iron chelating model molecule to mimick the iron state in physiological media had to be found. Used as a model of citrate, nitrilotriacetic acid (NTA) is among the most studied organic chelators. In our study, NTA was used with the aim to mimick the biological environment conditions, and the adopted strategy allowed to stabilize Fe(III) under quasi-physiological conditions (*i.e.*, pH 7.4 and citrate model). As said previously, DFoB is by far the chelating agent which has a much more powerful Fe(III) chelating constant (log $K_{Fe(III)DFoB}$ = 30; pFe = 26.5)[8] than NTA (log K_{FeNTA} ~15-16; pFe = 17.8)[52] favoring Fe(III) exchange. In the following experiments, FeNTA were therefore incubated with DFoB-STMS and key parameters characterizing the metal capture : capture capacity ($nmol.mg^{-1}$), capture efficiency (%) and molecular coverage of the DFOB chelate (%) were then evaluated as a function of time (kinetics). Stoichiometry of the exchange reaction was established by calculating the Fe/DFoB ratio.

$$\textbf{Capture Capacity} = \frac{n_{\text{Fe-captured}}\ (\text{nmol})}{m_{\text{silica}}\ (\text{mg})}$$

$$\textbf{Capture Efficiency} = \frac{n_{\text{Fe-captured}}\ (\text{mol})}{n_{\text{Fe initial}}\ (\text{mol})} \times 100$$

$$\textbf{DFoBgrafted Coverage} = \frac{n_{\text{Fer-captured}}\ (\text{mol})}{n_{\text{DFoB available}}\ (\text{mol})} \times 100$$

Ligand exchange kinetics

When DFoB is grafted at the surface of STMS NPs, the Fe(III) uptake kinetics by ligand exchange between FeNTA and DFoB-STMS could be slower compared to free DFoB. At pH 7.4, only $[FeNTA(OH)]^-$ species is reactive and follows a dissociative interchange mechanism of the Eigen−Wilkins type - independent of the nature of the binding ligand- with $k_{[FeNTA(OH)]-}$ values in the order of 10^4 M^{-1} s^{-1}.[38] Supernatants containing remaining FeNTA have been analyzed directly by UV-visible absorption spectrophotometry (λ_{max} = 270 nm). However, in our experimental conditions (HEPES buffer at 50 mM), the FeNTA absorption was markedly altered by another more intense absorption at about 210 nm (linked to HEPES) which prevents the accurate determination of the iron content (**Figure S4.A**). To overcome this problem and analyze FeNTA supernatants, free DFoB was added to the supernatant, which rapidly led to the formation of FeDFoB complex which is

characterized by a Ligand-to-Fe(III) charge transfer band (*i.e.*, LMCT) of moderate intensity centered at 430 nm (ε^{430} = 2950 $M^{-1}\cdot cm^{-1}$)[53]. The color changes from light yellow to orange, confirming the exchange of the ligands and the formation of the FeDFoB complex. To ensure more accurate determination of FeNTA using free DFoB, an absorption titration of FeNTA by DFoB was then undertaken, and the absorbance values at 430 nm were plotted as a function of DFoB concentrations (**Figure S4.B**). Hence, the ligand exchange was shown to be rapid and confirmed the stoichiometry of the reaction (FeNTA:DFoB 1:1).

A kinetic exchange study between FeNTA and DFoB-STMS in HEPES buffer at pH 7.4 was carried out. The mixture (FeNTA:$DFoB_{grafted}$ at a ratio of 0.85:1: at 25°C) was stirred for different reaction times (from 30 min to 1 day) and then centrifuged at 10 000 g. The supernatants were then analyzed using UV-visible absorption spectrophotometry using free DFoB in excess to ensure an accurate determination of the free iron contents.

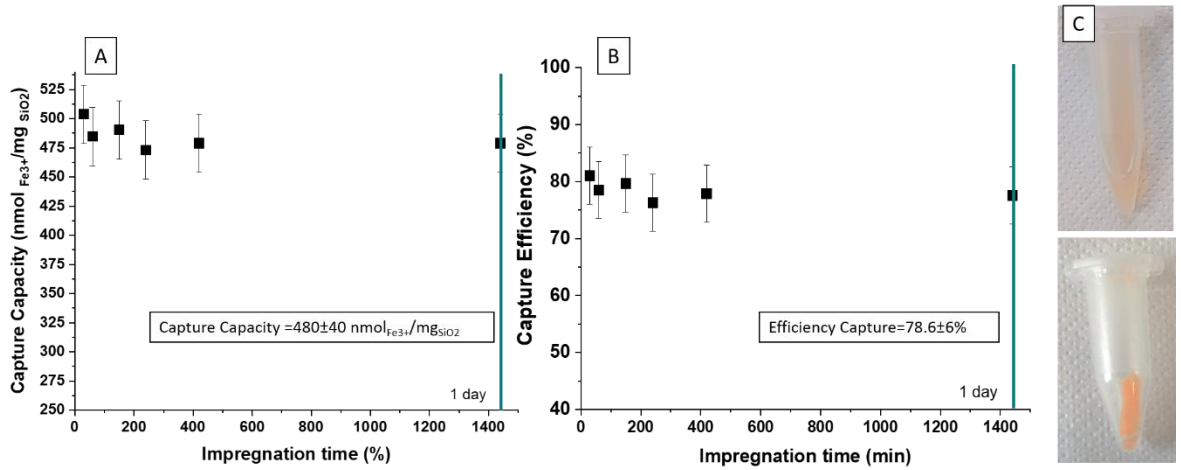

Figure 4. A) Capture capacity and B) capture efficiency of iron(III) by DFoB-STMS using different impregnation times for a ratio FeNTA:$DFoB_{grafted}$ of 0.85:1 at 25°C, pH 7.4. C) Pictures showing the orange colored suspension (top) and the centrifuged Fe-DFoB-STMS (bottom).

As shown on **Figure 4**, the values of the capture capacity and efficiency did not significantly changed over a 24 hours period with a maximum value reached after 30 minutes of contact of DFoB-STMS with FeNTA. According to these data, the metal exchange between FeNTA and DFoB-STMS can therefore be considered as fast, which is a major advantage for the development of any metal ion removal process. Nevertheless, we were unable to reduce the contact time to less than 30 minutes due to the experimental set-up (*i.e.,* centrifugation, washing, measurement of residual FeNTA content by absorption spectrophotometry). In average over this time period, the capture capacity of DFoB-STMS was calculated to be 480 $nmol_{Fe}\cdot mg_{SiO2}^{-1}$ (*i.e.*, 27 $\mu g_{Fe}\cdot mg_{SiO2}^{-1}$), which corresponds to a capture efficiency of *ca*. 78 % and a coverage of $DFoB_{grafted}$ molecules of *ca*. 66 %. These results are higher to those of other studies conducted with DFoB grafted onto other materials such as nanogel-

DFoB, which allow a capture efficiency of 50 % *in vivo* with ferritine (*i.e.,* universal intracellular protein that ensures iron storage) as a source of iron[54]*.* An other comparison can be done with mesoporous silica type MCM-41 functionalized with DFoB that allows a capture efficiency of ca. 60 % from FeEDTA used as a metal source[55].

The capture of Fe(III) was also confirmed by analyzing iron within the DFOB-STMS by TEM-EDX. First, TEM images of the FeDFoB-STMS showed the presence of an organic-like coating all around the STMS NPs, confirming a homogenous grafting of DFoB on the STMS (more than 40% wt by TGA) **(Figure 5.A and B** in low and high magnifications). EDX analysis in low and high magnification areas allowed detecting te presence of iron (attribution Fe-Kα 6.27 and Fe-Kβ 7.1 keV for the most intensive pics) and silicon (attribution 1.71 keV) atoms and determining a Fe/Si fraction of *ca.* 2 %. Noteworthy, EDX is a suitable method to detect the presence of such elements however it is not adapted to quantify with precision these elements as the TEM grids used in the preparation may contain silica and the error deviation related to EDX measurements is not negligible at low element % amounts.

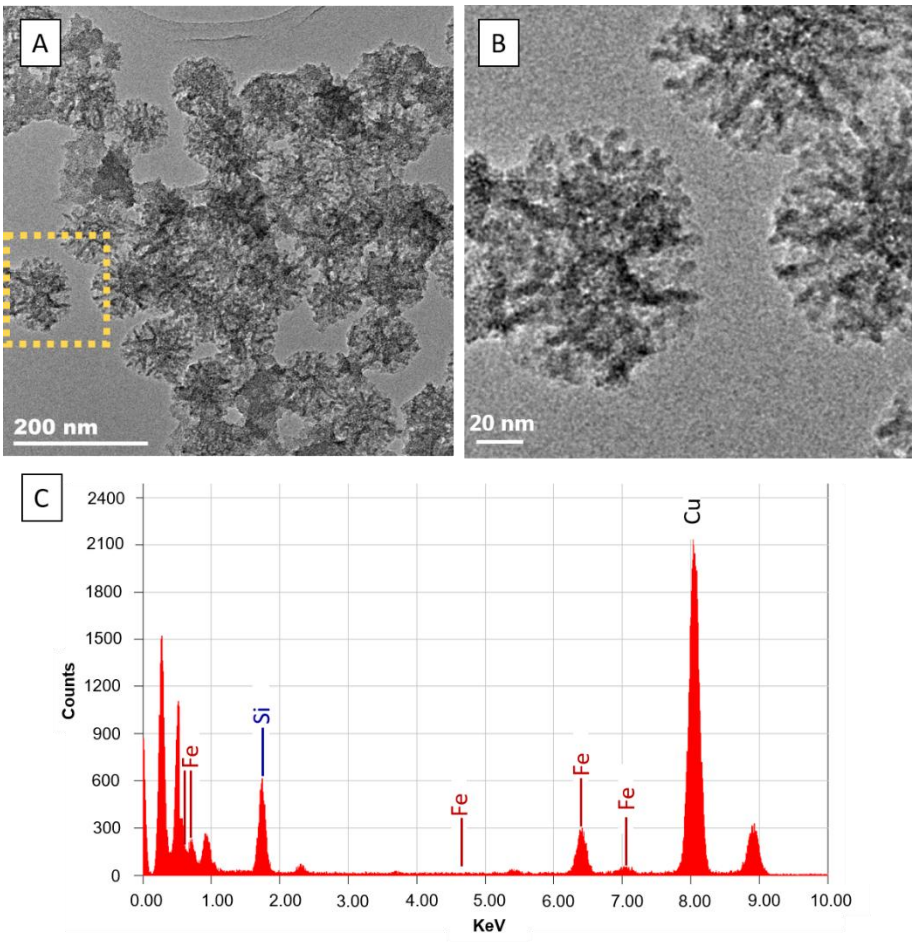

Figure 5. TEM images of FeDFoB-STMS with A) low magnification and B) high magnifications and C) EDX analysis of FeDFoB-STMS NPs.

Iron uptake for different FeNTA:DFoB$_{grafted}$ ratios and at different surface modifications steps

The capacity uptake of DFoB-STMS suspensions was then measured for different FeNTA:DFoB$_{grafted}$ molar ratios of 0.17, 0.85 and 1.7. The influence of the nature (*i.e.* coating) of the STMS surface: (bare) STMS, APTES-STMS or COOH-STMS was also evaluated as a control in this study to evaluate the impact of the supporting system (STMS) and the surface coating (naked, APTES or COOH grafting) on the Fe(III) loading (**Figure 6.A and B**).

For the three molar ratios, the results of **Figure 6.A and B.** (yellow curves) displayed the capture capacity and efficiency of our system under different FeNTA concentrations. Over these molar ratio range, the capture capacity normally increased from 32 to 799 nmol$_{Fe}$·mg^{-1}$_{STMS}$, while the capture efficiency increased to reach values of 67% and 65% at stoichiometries of 0.85 and 1.7:1 (i.e., STMS-DFOB has removed more than 65% of initially introduced iron). Regarding the coverage of DFoB molecules, **Figure 6. C** shows that the molecular coverage of the DFOB increases importantly from 4% for 0.17:1 stoichiometry, to 58 % for 0.85:1 stoichiometry and reaches finally a coverage of 109 % for 1.7:1 stoichiometry. This last result over 100% at 1.7 equivalent FeNTA, suggests strongly that in addition to a full occupation of the DFOB ligands by Fe(III), an additional binding of FeNTA occurs at the surface of the STMS NPs.

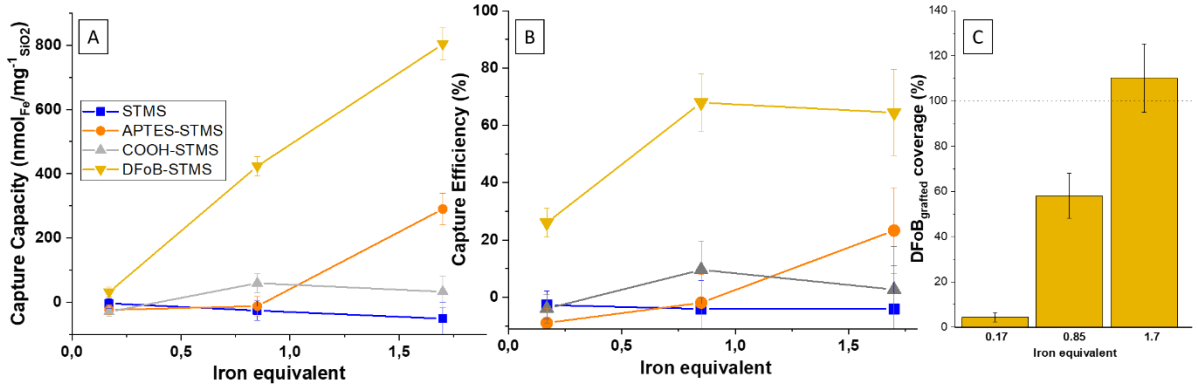

Figure 6 A) Capture capacities and B) efficiencies of STMS (blue), APTES-STMS (orange), COOH-STMS (gray) and DFoB-STMS (yellow) for different FeNTA:DFoB$_{grafted}$ ratios (0.17:1, 0.85:1 and 1.7 :1) with contact time of 30 minutes at 25°C, pH 7.4. C) Coverage represents the percentage of DFoB molecules occupied by Fe^{3+} cations. Experiments were repeated three times.

Hence, it could be assumed that parts of the silica surface that are not functionalized with DFoB have a significant effect on the iron (FeNTA) storage. The grafting process of the different steps has probably left other functions (APTES and COOH) that could potentially bind FeNTA**.** On this last point, the blue and grey curves show that STMS and COOH-STMS are not prone to efficient iron storage (less than 60 nmol·mg^{-} STMS), whereas iron capture seems to increase significantly with APTES-STMS at a 1.7:1 stoichiometry and thus reach a significant amount of FeNTA loaded with 290 nmol·mg^{-1}

APTES-STMS **(Figure 6.A)**. At physiological pH, FeNTA can be written as $[Fe^{III}(CO_2CH_3)_3N.H_2O.OH]^-$ and is negatively charged. As the pK_a of APTES-STMS is *ca*. 8, the surface is therefore partially positively charged at pH 7.4, and the amount of FeNTA adsorbed (orange curve) can be explained by electrostatic interactions between the positively charged surface and the negatively charged Fe(III) complex. Contrary, STMS and COOH-STMS are negatively charged at their surface at pH 7.4 and repulsive effects can explain the low capacities observed for these solids. It should be noted that this electrostatic interactions with grafted APTES onto silica NPs has already been described by Wu et al.[56], who captured negative $CuEDTA^{2-}$ and $CuHEDTA^-$ complexes. To summarize, the trend observed in iron(III) capture by DFOB-STMS can be explained by two mechanisms: one likely corresponds to strong and selective chelation binding with metal-ligand coordination bonds as a main ligand exchange process, and the other, non-specific and probably electrostatic in nature, could involve weaker binding of negatively charged FeNTA complexes onto residual positively charged surface (APTES-STMS).

Iron selectivity of the DFoB-STMS suspensions over other cations

The understanding and measurement of selectivity is a key factor to ensure a safe uptake of iron(III) and a high selectivity of the DFoB-STMS suspensions for iron (III) is an important property to consider for the biological applications of this nanoplatform. Iron capture should not be accompanied by a loss of other ions essential to the organism (i.e. Cu^{2+}, Zn^{2+}, Ca^{2+}). In this study, the chelation selectivity of Fe(III) with respect to other important cations of biological interest such as Al^{3+}, Zn^{2+}, Cu^{2+}, Ca^{2+} or Na^+ was evaluated. Indeed, blood is a complex system composed of numerous metal ions essential to the body's functioning. So, establishing whether DFoB-STMS NPs are able of selectively capturing iron(III) in a complex multi-element environment is essential. Two different media were used to demonstrate that DFoB-STMS can selectively capture iron: a multi-element system consisting of a solution containing different biological cations at the same initial concentration, and the Barth's solution consisting in a preparation which mimicks the ionic brain composition. Results are summarized in the next table (**Table 1**).

Table 1 Capture capacity and efficiency of DFoB-STMS with the two different solutions containing different metal cations. Parameters are : 0.95:1 FeNTA:$DFoB_{grafted}$ ratio, contact time of 30 minutes at 25°C, pH 7.4 and 7.7 mg of DFOB functionalized STMS. Experiment were performed in duplicate. *A NaOH (2M) solution was used to set the pH.

	Ion	Fe^{3+}	Mg^{2+}	Ca^{2+}	Al^{3+}	Zn^{2+}	K^{+}	Na^{+}
Multielement solution	**Initial concentration (mM)**	0.27±0.03					x	1.159*
	Capture Capacity ($nmol_{ion}/mg_{SiO2}$)	229±4.3	6.6±4.9	1.2±0.7	169±2.3	9.0±1.0	x	155±14
	Capture Efficiency (%)	44.2±1.6	1.1±1.5	0.9±1.3	32.9±0.9	1.9±0.4	x	6.8±1.2
Barth's buffer	**Initial concentration (mM)**	0.29	0.82	1.32	x	0.04	1.89	90
	Capture Capacity ($nmol_{ion}/mg_{SiO2}$)	428±3.6	174±19.2	437±75	x	9.±3.6	367±1.8	4293±13
	Capture Efficiency (%)	69.2±1.2	8.2±1.7	13.4±4.5	x	8.8±8.2	1.5±0.1	1.9±0.1
log $K_{Ion\text{-}DFoB}$		30	9[51]	3[51]	24.5[9]	10.1[11]	/	/

For the multielement solution, the capture capacity and efficiency of iron are lower than in the previous experiments, which is explained mainly by competition between Al^{3+} and Fe^{3+} cations. As compared to the previous study (**Figure 4**) without any competing cation (*i.e.*, capture capacity of 480 $nmol_{Fe3+}\cdot mg_{SiO2}$ and efficiency of *ca*. 78% at a stoichiometry FeNTA:$DFOB_{grafted}$ 0.85:1), the results showed a significant reduction in iron capture (*i.e.*, capture capacity of 229 $nmol_{Fe3+}\cdot mg_{SiO2}^{-1}$ and efficiency *ca*. 44% at a stochiometry FeNTA:$DFOB_{grafted}$ 0.95:1). Indeed, Al^{3+} and Fe^{3+} cations have comparable coordination properties and high complexation constants with DFoB (*i.e.*, log K_{MDFoB} = 30 and 24.5 for Fe^{3+} and Al^{3+}, respectively). Even though the stability constant is higher for FeDFoB, Al^{3+} can competes and distributes within the grafted DFoB. It is noteworthy that the sum of the capture efficiencies for Fe^{3+} and Al^{3+} (*ca.* 77%) is in excellent agreement with that determined from the experiment conducted in absence of any competing metal ions (*ca.* 78%). Concerning the other competing cations Mg^{2+}, Ca^{2+} and Zn^{2+}, their captures were found to be less important, in agreement with the much lower stability constants of the corresponding complexes. As far as Na^{+} and K^{+} ions are concerned, no data could be found with DFoB in terms of stability. These adsorption could be possible because, as described before, electrostatic interactions between cations and COOH grafting and naked STMS can occur. In previous works, studies were performed concerning this phenomenon:

COOH functionnalization was already used for metallic cations capture[57,58] which were also demonstrated to be attracted by the negative silica surface[59].

Regarding the study with the Barth's solution mimicking the ionic brain composition, where the concentrations of the biological cations (Mg^{2+}, Ca^{2+}, Zn^{2+} and Na^{+}) are higher than that of Fe^{3+} set to 0.29 mM (see **Table 1**, Barth's buffer line), values obtained for iron capture capacity and efficiency (428 $nmol_{Fe3+}\cdot mg_{SiO2}^{-1}$ and 69%) were found relatively close to the results obtained in the previous kinetic and stoechiometric studies (480 $nmol_{Fe3+}\cdot mg_{SiO2}^{-1}$ and 78 %). As the Barth's aqueous buffer does not present any Al^{3+} cation, a close relationship can be clearly highlighted on the ability of DFOB-STMS to efficiently chelate and capture iron in the presence or not of aluminium cation. Regarding the capture capacities for the other cations having I or II valency (Mg^{2+}, Ca^{2+}, Zn^{2+} and Na^{+}), although their capture capacities are quite high, their capture efficiencies remain however low without being negligible, indicating that the homeostatic levels of these cations could be slightly or moderately affected during the selective iron capture. For further investigations, it would be necessary to ensure that the homeostatic levels of these cations remain stable for the safety of such treatment because depletion of some relevant ions could be risky, *i.e.,* a depletion of sodium could produce cardiovascular problems as hypotension episodes[60].

Conclusion

In this work, a new nanoplatform efficient for iron removal from complex biological media has been designed. It consists of original mesoporous silica with a large pore stellate morphology on which an iron chelating agent of natural origin has been anchored. The synthesis of such stellate silica has been reported recently and their use in decontamination has never been investigated up to now. By considering the challenges and the targeted application which is the specific removal of iron from a biological medium, desferrioxamine B (DFoB) chelator, already used in its free form for iron capture in body, was also found herein highly relevant when covalently immobilized on stellate silica to efficiently and selectively extract iron(III) alone in solution or combined to a mixture of biological relevant cations.

As compared to the findings in the litterature, the use of DFOB-STMS offers key advantages:

- Large pore stellate silica NPs are prepared according to a straightforward and reproducible procedure, while chelating DFoB ligands afforded selective iron capture moiety and very stable complexes.
- The grafting of DFoB, to modify the surface of homogeneous stellate silica NPs, was successfully achieved and controlled. It leads to a great coverage of the chelator of 730 $nmol\cdot mg^{-1}$ (*i.e.,* 0.85 ligand·per nm^2).

- The DFOB-STMS are able to capture very fast (in less than 30 minutes) a high amount of iron(III) up to a capture capacity of 480 $nmol_{Fe3+}/mg_{SiO2}$ with a good uptake efficiency (*ca.* 78%) meaning that 78 % of the initial iron is uptaken for a stoichiometry 0.85:1 (FeNTA : DFoB);
- Comparison of the iron uptake by our DFoB-STMS with other surface modification (bare, APTES, COOH) indicates that iron capture of our DFoB-STMS is mainly due to chelation while the other surfaces have slight or moderate non-specific adsorption;
- At last, about the metal selectivity, studies in two different multielement media, showed a high selectivity for iron(III) over other metal ions. For a multielement solution mimicking the extracellular brain ionic composition (Barth's buffer), the iron capture was found to be close to that performed in the absence of competing ions (capture capacity of 428 $nmol_{Fe}{\cdot}mg_{SiO2}^{-1}$and capture efficiency of *ca*. 69 %) while in the presence of Al^{3+} that strongly competes with Fe^{3+}, the capture of iron decreased (capture capacity 229 $nmol_{Fe}{\cdot}mg_{SiO2}^{-1}$ and capture efficiency of *ca.* 44 %). Due to their closely related properties, Al^{3+} and Fe^{3+} thermodynamically distribute within the DFoB-STMS (capture efficiency of *ca.* 77% for both Al^{3+} and Fe^{3+}).

Hence, such works may pave the way towards new nanosystems at the interface between depollution and nanomedecine. Future experiments will aim to investigate such nanoplatforms with other chelating agents to demonstrate the versatility of this design and approach for other biomedical issues. The introduction of a magnetic core will be also assessed to offer possibility of magnetic recovery of such new nanoplatforms.

Aknowledgements.

This material is based on research supported by the Asian Office of Aerospace Research and Development (AOARD), Grant # FA2386-17-1-4051. The AOARD and the region Grand Est are thanked for the PhD funding of P.D.R. M. E. thank the CNRS and the University of Strasbourg (LIMA UMR 7042) for financial support.

Bibliography

(1) Sharma, S. K.; Petrusevski, B.; Schippers, J. C. Biological Iron Removal from Groundwater: A Review. *J. Water Supply Res. Technol.-Aqua* **2005**, *54* (4), 239–247.
(2) Puig, S.; Ramos-Alonso, L.; Romero, A. M.; Martínez-Pastor, M. T. The Elemental Role of Iron in DNA Synthesis and Repair. *Met. Integr. Biometal Sci.* **2017**, *9* (11), 1483–1500.
(3) Buffet, C. L'hémochromatose à l'heure de la génétique. *Presse Médicale* **2007**, *36* (9, Part 2), 1269–1270.
(4) Westlin, W. F. Deferoxamine in the Treatment of Acute Iron Poisoning: Clinical Experiences with 172 Children. *Clin. Pediatr. (Phila.)* **1966**, *5* (9), 531–535.

(5) Brittenham, G. M.; Griffith, P. M.; Nienhuis, A. W.; McLaren, C. E.; Young, N. S.; Tucker, E. E.; Allen, C. J.; Farrell, D. E.; Harris, J. W. Efficacy of Deferoxamine in Preventing Complications of Iron Overload in Patients with Thalassemia Major. *N. Engl. J. Med.* **1994**, *331* (9), 567–573.
(6) Ihnat, P. M.; Vennerstrom, J. L.; Robinson, D. H. Solution Equilibria of Deferoxamine Amides. *J. Pharm. Sci.* **2002**, *91* (7), 1733–1741.
(7) Kornreich-Leshem, H.; Ziv, C.; Gumienna-Kontecka, E.; Arad-Yellin, R.; Chen, Y.; Elhabiri, M.; Albrecht-Gary, A.-M.; Hadar, Y.; Shanzer, A. Ferrioxamine B Analogues: Targeting the FoxA Uptake System in the Pathogenic Yersinia Enterocolitica. *J. Am. Chem. Soc.* **2005**, *127* (4), 1137–1145.
(8) Farkas, E.; Enyedy, É. A.; Csóka, H. A Comparison between the Chelating Properties of Some Dihydroxamic Acids, Desferrioxamine B and Acetohydroxamic Acid. *Polyhedron* **1999**, *18* (18), 2391–2398.
(9) Evers, A.; Hancock, R. D.; Martell, A. E.; Motekaitis, R. J. Metal Ion Recognition in Ligands with Negatively Charged Oxygen Donor Groups. Complexation of Iron(III), Gallium(III), Indium(III), Aluminum(III), and Other Highly Charged Metal Ions. *Inorg. Chem.* **1989**, *28* (11), 2189–2195.
(10) Anderegg, G.; L'Eplattenier, F.; Schwarzenbach, G. Hydroxamatkomplexe III. Eisen(III)-Austausch Zwischen Sideraminen Und Komplexonen. Diskussion Der Bildungskonstanten Der Hydroxamatkomplexe. *Helv. Chim. Acta* **1963**, *46* (4), 1409–1422.
(11) Farkas, E.; Csóka, H.; Micera, G.; Dessi, A. Copper(II), Nickel(II), Zinc(II), and Molybdenum(VI) Complexes of Desferrioxamine B in Aqueous Solution. *J. Inorg. Biochem.* **1997**, *65* (4), 281–286.
(12) Bergeron, R. J.; Wiegand, J.; Brittenham, G. M. HBED: A Potential Alternative to Deferoxamine for Iron-Chelating Therapy. *Blood* **1998**, *91* (4), 1446–1452.
(13) Olivieri, N. F.; Brittenham, G. M. Iron-Chelating Therapy and the Treatment of Thalassemia. *Blood* **1997**, *89* (3), 739–761.
(14) Piga, A.; Galanello, R.; Forni, G. L.; Cappellini, M. D.; Origa, R.; Zappu, A.; Donato, G.; Bordone, E.; Lavagetto, A.; Zanaboni, L.; Sechaud, R.; Hewson, N.; Ford, J. M.; Opitz, H.; Alberti, D. Randomized Phase II Trial of Deferasirox (Exjade, ICL670), a Once-Daily, Orally-Administered Iron Chelator, in Comparison to Deferoxamine in Thalassemia Patients with Transfusional Iron Overload. *Haematologica* **2006**, *91* (7), 873–880.
(15) Liu, G.; Men, P.; Perry, G.; Smith, M. A. Nanoparticle and Iron Chelators as a Potential Novel Alzheimer Therapy. *Methods Mol. Biol. Clifton NJ* **2010**, *610*, 123–144.
(16) Farjadian, F.; Ghasemi, S.; Heidari, R.; Mohammadi-Samani, S. In Vitro and in Vivo Assessment of EDTA-Modified Silica Nano-Spheres with Supreme Capacity of Iron Capture as a Novel Antidote Agent. *Nanomedicine Nanotechnol. Biol. Med.* **2017**, *13* (2), 745–753.
(17) Kefeni, K. K.; Mamba, B. B.; Msagati, T. A. M. Application of Spinel Ferrite Nanoparticles in Water and Wastewater Treatment: A Review. *Sep. Purif. Technol.* **2017**, *188*, 399–422.
(18) Reddy, D. H. K.; Yun, Y.-S. Spinel Ferrite Magnetic Adsorbents: Alternative Future Materials for Water Purification? *Coord. Chem. Rev.* **2016**, *315*, 90–111.
(19) Pratsinis, A.; Zuercher, S.; Forster, V.; Fischer, E. J.; Luciani, P.; Leroux, J.-C. Liposome-Supported Enzymatic Peritoneal Dialysis. *Biomaterials* **2017**, *145*, 128–137.
(20) Khajeh, M.; Laurent, S.; Dastafkan, K. Nanoadsorbents: Classification, Preparation, and Applications (with Emphasis on Aqueous Media). *Chem. Rev.* **2013**, *113* (10), 7728–7768.
(21) Adeleye, A. S.; Conway, J. R.; Garner, K.; Huang, Y.; Su, Y.; Keller, A. A. Engineered Nanomaterials for Water Treatment and Remediation: Costs, Benefits, and Applicability. *Chem. Eng. J.* **2016**, *286*, 640–662.
(22) Khin, M. M.; Nair, A. S.; Babu, V. J.; Murugan, R.; Ramakrishna, S. A Review on Nanomaterials for Environmental Remediation. *Energy Environ. Sci.* **2012**, *5* (8), 8075–8109.
(23) Simeonidis, K.; Mourdikoudis, S.; Kaprara, E.; Mitrakas, M.; Polavarapu, L. Inorganic Engineered Nanoparticles in Drinking Water Treatment: A Critical Review. *Environ. Sci. Water Res. Technol.* **2016**, *2* (1), 43–70.
(24) Yang, J.; Hou, B.; Wang, J.; Tian, B.; Bi, J.; Wang, N.; Li, X.; Huang, X. Nanomaterials for the Removal of Heavy Metals from Wastewater. *Nanomaterials* **2019**, *9* (3), 424.

(25) Zhang, X.; Niu, H.; Pan, Y.; Shi, Y.; Cai, Y. Chitosan-Coated Octadecyl-Functionalized Magnetite Nanoparticles: Preparation and Application in Extraction of Trace Pollutants from Environmental Water Samples. *Anal. Chem.* **2010**, *82* (6), 2363–2371.
(26) Cashin, V. B.; Eldridge, D. S.; Yu, A.; Zhao, D. Surface Functionalization and Manipulation of Mesoporous Silica Adsorbents for Improved Removal of Pollutants: A Review. *Environ. Sci. Water Res. Technol.* **2018**, *4* (2), 110–128.
(27) Vallet-Regí, M.; Ruiz-González, L.; Izquierdo-Barba, I.; M. González-Calbet, J. Revisiting Silica Based Ordered Mesoporous Materials: Medical Applications. *J. Mater. Chem.* **2006**, *16* (1), 26–31.
(28) Wells, C.; Vollin-Bringel, O.; Fiegel, V.; Harlepp, S.; Schueren, B. V. der; Bégin-Colin, S.; Bégin, D.; Mertz, D. Engineering of Mesoporous Silica Coated Carbon-Based Materials Optimized for an Ultrahigh Doxorubicin Payload and a Drug Release Activated by PH, T, and NIR-Light. *Adv. Funct. Mater.* **2018**, *28* (17), 1706996.
(29) Ménard, M.; Meyer, F.; Parkhomenko, K.; Leuvrey, C.; Francius, G.; Bégin-Colin, S.; Mertz, D. Mesoporous Silica Templated-Albumin Nanoparticles with High Doxorubicin Payload for Drug Delivery Assessed with a 3-D Tumor Cell Model. *Biochim. Biophys. Acta BBA - Gen. Subj.* **2019**, *1863* (2), 332–341.
(30) Fu, C.; Liu, T.; Li, L.; Liu, H.; Chen, D.; Tang, F. The Absorption, Distribution, Excretion and Toxicity of Mesoporous Silica Nanoparticles in Mice Following Different Exposure Routes. *Biomaterials* **2013**, *34* (10), 2565–2575.
(31) Hakami, O.; Zhang, Y.; Banks, C. J. Thiol-Functionalised Mesoporous Silica-Coated Magnetite Nanoparticles for High Efficiency Removal and Recovery of Hg from Water. *Water Res.* **2012**, *46* (12), 3913–3922.
(32) Heidari, A.; Younesi, H.; Mehraban, Z. Removal of Ni(II), Cd(II), and Pb(II) from a Ternary Aqueous Solution by Amino Functionalized Mesoporous and Nano Mesoporous Silica. *Chem. Eng. J.* **2009**, *153* (1), 70–79.
(33) Li, G.; Zhao, Z.; Liu, J.; Jiang, G. Effective Heavy Metal Removal from Aqueous Systems by Thiol Functionalized Magnetic Mesoporous Silica. *J. Hazard. Mater.* **2011**, *192* (1), 277–283.
(34) Dindar, M. H.; Yaftian, M. R.; Rostamnia, S. Potential of Functionalized SBA-15 Mesoporous Materials for Decontamination of Water Solutions from Cr(VI), As(V) and Hg(II) Ions. *J. Environ. Chem. Eng.* **2015**, *3* (2), 986–995.
(35) Sangvanich, T.; Sukwarotwat, V.; Wiacek, R. J.; Grudzien, R. M.; Fryxell, G. E.; Addleman, R. S.; Timchalk, C.; Yantasee, W. Selective Capture of Cesium and Thallium from Natural Waters and Simulated Wastes with Copper Ferrocyanide Functionalized Mesoporous Silica. *J. Hazard. Mater.* **2010**, *182* (1), 225–231.
(36) Chang, C.-Y.; Chau, L.-K.; Hu, W.-P.; Wang, C.-Y.; Liao, J.-H. Nickel Hexacyanoferrate Multilayers on Functionalized Mesoporous Silica Supports for Selective Sorption and Sensing of Cesium. *Microporous Mesoporous Mater.* **2008**, *109* (1), 505–512.
(37) Zhang, K.; Xu, L.-L.; Jiang, J.-G.; Calin, N.; Lam, K.-F.; Zhang, S.-J.; Wu, H.-H.; Wu, G.-D.; Albela, B.; Bonneviot, L.; Wu, P. Facile Large-Scale Synthesis of Monodisperse Mesoporous Silica Nanospheres with Tunable Pore Structure. *J. Am. Chem. Soc.* **2013**, *135* (7), 2427–2430.
(38) Martin-Benlloch, X.; Haid, S.; Novodomska, A.; Rominger, F.; Pietschmann, T.; Davioud-Charvet, E.; Elhabiri, M. Physicochemical Properties Govern the Activity of Potent Antiviral Flavones. *ACS Omega* **2019**, *4* (3), 4871–4887.
(39) Anderegg, G. Critical Survey of Stability Constants of NTA Complexes. *Pure Appl. Chem.* **1982**, *54* (12), 2693–2758.
(40) Wolsey, W. C. Perchlorate Salts, Their Uses and Alternatives. *J. Chem. Educ.* **1973**, *50* (6), A335.
(41) Bastian, Robert.; Weberling, Richard.; Palilla, Frank. Determination of Iron by Ultraviolet Spectrophotometry. *Anal. Chem.* **1956**, *28* (4), 459–462.
(42) Budimir, A.; Humbert, N.; Elhabiri, M.; Osinska, I.; Biruš, M.; Albrecht-Gary, A.-M. Hydroxyquinoline Based Binders: Promising Ligands for Chelatotherapy? *J. Inorg. Biochem.* **2011**, *105* (3), 490–496.

(43) Perton, F.; Harlepp, S.; Follain, G.; Parkhomenko, K.; Goetz, J. G.; Bégin-Colin, S.; Mertz, D. Wrapped Stellate Silica Nanocomposites as Biocompatible Luminescent Nanoplatforms Assessed in Vivo. *J. Colloid Interface Sci.* **2019**, *542*, 469–482.
(44) Zhang, K.; Chen, H.-L.; Albela, B.; Jiang, J.-G.; Wang, Y.-M.; He, M.-Y.; Bonneviot, L. High-Temperature Synthesis and Formation Mechanism of Stable, Ordered MCM-41 Silicas by Using Surfactant Cetyltrimethylammonium Tosylate as Template. *Eur. J. Inorg. Chem.* **2011**, *2011* (1), 59–67.
(45) Cui, X.; Zin, W.-C.; Cho, W.-J.; Ha, C.-S. Nonionic Triblock Copolymer Synthesis of SBA-15 above the Isoelectric Point of Silica (PH=2–5). *Mater. Lett.* **2005**, *59* (18), 2257–2261.
(46) Stöber, W.; Fink, A.; Bohn, E. Controlled Growth of Monodisperse Silica Spheres in the Micron Size Range. *J. Colloid Interface Sci.* **1968**, *26* (1), 62–69.
(47) Wang, X.-Y.; Mertz, D.; Blanco-Andujar, C.; Bora, A.; Ménard, M.; Meyer, F.; Giraudeau, C.; Bégin-Colin, S. Optimizing the Silanization of Thermally-Decomposed Iron Oxide Nanoparticles for Efficient Aqueous Phase Transfer and MRI Applications. *RSC Adv.* **2016**, *6* (96), 93784–93793.
(48) Schiestel, T.; Brunner, H.; Tovar, G. E. M. Controlled Surface Functionalization of Silica Nanospheres by Covalent Conjugation Reactions and Preparation of High Density Streptavidin Nanoparticles. *J. Nanosci. Nanotechnol.* **2004**, *4* (5), 504–511.
(49) An, Y.; Chen, M.; Xue, Q.; Liu, W. Preparation and Self-Assembly of Carboxylic Acid-Functionalized Silica. *J. Colloid Interface Sci.* **2007**, *311* (2), 507–513.
(50) An, Y.; Chen, M.; Xue, Q.; Liu, W. Preparation and Self-Assembly of Carboxylic Acid-Functionalized Silica. *J. Colloid Interface Sci.* **2007**, *311* (2), 507–513.
(51) Kiss, T.; Farkas, E. Metal-Binding Ability of Desferrioxamine B. *J. Incl. Phenom. Mol. Recognit. Chem.* **1998**, *32* (2), 385–403.
(52) Elhabiri, M.; Carrër, C.; Marmolle, F.; Traboulsi, H. Complexation of Iron(III) by Catecholate-Type Polyphenols. *Inorganica Chim. Acta* **2007**, *360* (1), 353–359.
(53) Kornreich-Leshem, H.; Ziv, C.; Gumienna-Kontecka, E.; Arad-Yellin, R.; Chen, Y.; Elhabiri, M.; Albrecht-Gary, A.-M.; Hadar, Y.; Shanzer, A. Ferrioxamine B Analogues: Targeting the FoxA Uptake System in the Pathogenic Yersinia Enterocolitica. *J. Am. Chem. Soc.* **2005**, *127* (4), 1137–1145.
(54) Wang, Y.; Liu, Z.; Lin, T.-M.; Chanana, S.; Xiong, M. P. Nanogel-DFO Conjugates as a Model to Investigate Pharmacokinetics, Biodistribution, and Iron Chelation in Vivo. *Int. J. Pharm.* **2018**, *538* (1), 79–86.
(55) Alberti, G.; Emma, G.; Colleoni, R.; Pesavento, M.; Marina Nurchi, V.; Biesuz, R. Novel DFO-Functionalized Mesoporous Silica for Iron Sensing. Part 2. Experimental Detection of Free Iron Concentration (PFe) in Urine Samples. *Analyst* **2014**, *139* (16), 3940–3948.
(56) Wu, L.; Wang, H.; Lan, H.; Liu, H.; Qu, J. Adsorption of Cu(II)–EDTA Chelates on Tri-Ammonium-Functionalized Mesoporous Silica from Aqueous Solution. *Sep. Purif. Technol.* **2013**, *117*, 118–123.
(57) Bensacia, N.; Fechete, I.; Moulay, S.; Debbih-Boustila, S.; Boos, A.; Garin, F. Removal of Cadmium (II) from Aqueous Media Using COOH/TUD-1 Mesoporous Solid. Kinetic and Thermodynamic Studies. *Environ. Eng. Manag. J.* **2014**, *13* (10), 2675–2686.
(58) Bensacia, N.; Fechete, I.; Moulay, S.; Hulea, O.; Boos, A.; Garin, F. Kinetic and Equilibrium Studies of Lead(II) Adsorption from Aqueous Media by KIT-6 Mesoporous Silica Functionalized with –COOH. *Comptes Rendus Chim.* **2014**, *17* (7), 869–880.
(59) Peng, L.; Qisui, W.; Xi, L.; Chaocan, Z. Zeta-Potentials and Enthalpy Changes in the Process of Electrostatic Self-Assembly of Cations on Silica Surface. *Powder Technol.* **2009**, *193* (1), 46–49.
(60) Kooman, J. P.; Sande, F. V. D.; Leunissen, K.; Locatelli, F. Editorials: Sodium Balance in Hemodialysis Therapy. *Semin. Dial.* **2003**, *16* (5), 351–355.